Thermal modeling of a large prismatic LiFePO4/graphite battery. Coupled thermal and heat generation models for characterization and simulation.

Nicolas Damay, Christophe Forgez, Marie-Pierre Bichat, Guy Friedrich

Thermal modeling of a large prismatic $LiFePO_4$/graphite battery. Coupled thermal and heat generation models for characterization and simulation

Nicolas Damay[a,b], Christophe Forgez[a,*], Marie-Pierre Bichat[b], Guy Friedrich[a]

[a] *Sorbonne universités, Université de technologie de Compiègne*
EA1006 Laboratoire Electromécanique
Centre de recherche Royallieu, CS 60319, 60203 Compiègne cedex (France)
[b] *E4V, 9 avenue Georges Auric, 72000 Le Mans (France)*

Abstract

This paper deals with the thermal modeling of a large prismatic Li-ion battery ($LiFePO_4$/graphite). A lumped model representing the main thermal phenomena in the cell, in and outside the casing, is hereby proposed. Most of the parameters are determined analytically using physical and geometrical properties. The heat capacity, the internal and the interfacial thermal resistances between the battery and its cooling system are experimentally identified. On the other hand, the heat sources modeling is considered to be one of the most difficult task. In order to overcome this problem, a heat generation model is included. More specifically, the electrical losses are computed thanks to an electrical model which is represented by an equivalent electric circuit. A method is also proposed for parameter determination which is based on a quasi-steady state assumption. It also takes into account the battery heating during characterization which is the temperature variation due to heat generation during current pulses. This temperature variation is estimated thanks to the coupled thermal and heat generation models. The electrical parameters are determined as function of state of charge (SoC), temperature and current. Finally, the proposed coupled models are experimentally validated with a precision of 1°C.

Keywords: Lithium-ion, Batteries, $LiFePO_4$, Thermal Modeling, Electrical Losses Modeling, Equivalent Electric Circuit.

1. Introduction

Energy management and security are key issues for electric and hybrid vehicles development. Many battery sizing criteria are linked to its thermal behavior (power requirement, autonomy, temperature limitations, life span). Thus, a thermal model is useful when it comes to battery and its cooling system optimization. During operation, Battery Management Systems (BMS) ensures the efficiency and the safety of the energy storage. By means of a thermal model, the BMS is able to estimate the internal temperature and to predict its evolution. Besides, this information can improve the accuracy of an electrical model, used to monitor the state of charge (SoC) or the state of health (SoH) [1, 2].

Several papers deal with the thermal modeling of battery, using different approaches such as Partial Differential Equation (PDE) [3] or Linear Parameter-Varying (LPV) models [4], finite element method (FEM) [5, 6, 7] or electrical equivalent circuit [8, 9]. Thermal parameters can be determined using analytical relations which need a previous knowledge of the battery [6, 10]. They can also be determined experimentally by adapting a model to experimental data [11, 12, 13].

The purpose of this work is to establish a model suitable for the on-board energy management of a battery pack. 3D thermal models (such as FEM) are well-suited for the battery design purpose, but they are not compatible with the low computational resources of micro-controllers used in BMS [5, 14]. Therefore, a thermal model of a large prismatic Li-ion battery ($LiFePO_4$/graphite) is proposed, based on an equivalent electrical circuit where the thermal parameters are determined using analytical and experimental methods.

Inside a prismatic battery pack, cell temperatures have been measured as quite homogeneous. The hottest elements appeared to be in the central location, making this position critical for life span and reliability. Consequently, this study focuses on modeling the battery pack central cell (40 Ah). A difference of about 0.2 °C has been measured between the latter and the neighboring cells. Since this thermal gradient is small, the central cell is assumed to expel its heat only through its base (see Figure 1). As a result, their cooling performances are strongly dependent on the interfacial thermal resistance between the base and the cooling system. This thermal resistance has to be determined experimentally, but as it has no thickness, it

*Corresponding author
Email address: christophe.forgez@utc.fr (Christophe Forgez)

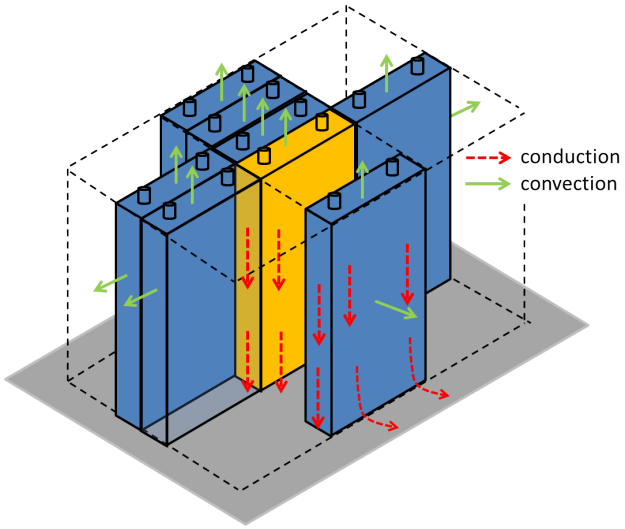

Figure 1: Prismatic cells (3x7) integration in battery pack, on a cooling plate (grey). White arrows represent cooling heat flows.

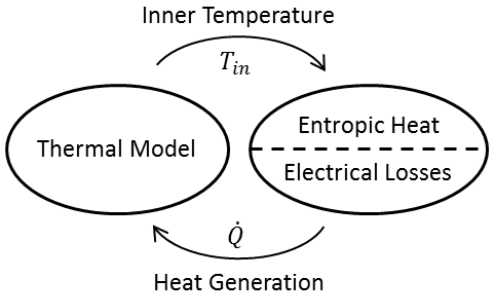

Figure 2: Coupled thermal and heat generation models.

cannot be measured using sensors. Therefore, it has to be determined indirectly.

For any battery thermal model, the heat sources are one of the most difficult components to represent, since they are highly non linear. Thus, a specific model is developed for heat generation, which computes both entropic heat and electrical losses, in relation to the inner temperature determined by the thermal model (Figure 2).

The entropic heat is usually modeled by means of an entropy-variation look-up table expressed as a function of the SoC. Its measurement is time-consuming, as the classical method requires approximately one day per SoC-operating point [15, 16]. Hence, several days, or even weeks, are necessary to obtain a high-resolution table. Interestingly, a new method has been recently proposed by Schmidt *et al.* [17], taking only several hours and giving very high resolution results.

Electrical losses are extracted from an electrical model of the battery which is strongly dependent on temperature, current, SoC and aging. Hence, they present a difficult task in terms of modeling. They can be estimated by solving electrochemical equations, but the latter requires the knowledge of many internal parameters, which are difficult to obtain [18, 19, 20]. Another approach is to use equivalent electrical circuits. The simplest one is a Thévenin equivalent circuit (whose single resistance eventually depends on temperature, current or SoC) [7, 21]. Dynamic models are also used, similar to Randles' circuit. Many studies achieved modeling of the diffusion phenomenon, which corresponds to the mass transport within the battery electrodes and electrolyte. It occurs at low frequencies (below 1 Hz) and depends on the considered chemistry. The electrical behavior of the diffusion phenomenon can be approximated by : a series RC circuit [22, 23, 24], constant phase elements (CPE) [24, 25] or non integer derivatives [26]. Moreover, the polarization (caused by a current) and the relaxation (in open-circuit) have different dynamics. Thus, a complete model should consider both case [27].

Regardless of the chosen method, any electrical model requires well-determined parameters. Their accurate determination is made difficult because of their sensibilities to SoC and temperature variations during tests, especially for low temperatures and high currents. One approach is to work in the frequency-domain, using electrochemical impedance spectroscopy (EIS) [26, 28]. They can also be determined in the time-domain, through current pulses [23, 24, 25]. These two approaches can be combined in order to reach a maximum precision [28].

In this paper, another equivalent electrical circuit is being proposed in order to model the battery electrical behavior, from which losses are computed. Its parameters are functions of temperature, current and SoC (aging is not considered in this study). Because the aim of this study is to model the heat generation, only the polarization behavior is characterized. Therefore, relaxation is assumed to behave like polarization and to generate no heat. The coupled thermal and heat generation models present the benefit of being able to compute the cell key-temperatures evolution, while being simple enough to be implemented in real time calculators.

In the first part, main thermal phenomena are modeled using a thermal network. Analytical and experimental methods for thermal parameters identification are presented. In the second part, heat sources are modeled and a method is proposed for electrical parameters determination. Finally, the experimental validation of the coupled models, through a discharge-charge cycle, is presented and discussed.

2. Thermal modeling

2.1. Model structure

A lumped thermal model [10] - also called equivalent electric circuit - has been used to model the studied cell. This approach is based on the formal analogy between thermal and electrical phenomena. Nodes are associated with volumes (assumed isothermal), capacitances represent heat accumulation, resistances represent heat transfers (by conduction, convection or radiation), current sources

represent heat generation and voltage sources represent set temperatures. Capacitances, current and voltage sources are used between a node and the ground node. In order to simplify the model representation on figures, set temperatures are written without the corresponding voltage source symbols.

In the studied application, cells have been integrated in a battery pack as shown in Figure 1. They are connected to a cooling system by their bases. Concerning the horizontal heat transfers, three configurations with different boundary conditions can be highlighted:

- **at the center**: heat may flow between cells by conduction;
- **on a side**: heat can flow between the cell and the battery pack inner atmosphere by convection through one face;
- **on a corner**: heat can flow between the cell and the battery pack inner atmosphere by convection through two faces.

The studied cell was modeled by the equivalent electric circuit shown on Figure 3, where there is one central node for the cell core, one node per face and one per terminal. This representation is able to stand for each of the three cell configurations. In this way, it anticipates the creation of a whole battery-pack model.

In the core: elements connected to the central node (green) stand for heat generation $\dot{Q}$, accumulation C and transfers (resistances with a "i" subscript). Because of the poor thermal contacts between the cell core and faces in y and z directions, heat transfers between them are neglected. Due to the foil stacking internal structure, the cell core can be considered having a homogeneous specific heat and an anisotropic thermal conductivity (being equal in y and z directions and different in the x direction) [6]. Despite its dimensions, the cell core is considered isothermal in y and z directions thanks to the current collectors. This has been confirmed via tests made by a third party. All core thermal properties are assumed to be constant regarding the SoC [11]. As for $R_{i,+}$ and $R_{i,-}$, they stand for conduction through the current collectors.

In the casing: resistances connecting the casing faces (red, with a "s" subscript) stand for heat transfers through the casing. All casing thermal capacities are neglected compared to the core heat capacity and no heat generation has been considered. Consequently, there are only heat transfers by conduction through the casing.

Outside the casing: outer elements (blue, with an "e" subscript) represent thermal exchanges between the cell and its environment (by conduction, convection and/or radiation, depending on the cell location in the battery pack). The resistance $R_{e,bot}$ below the cell represents the contact resistance between the cell base and the cooling system. Other resistances represent heat exchanges, by the lateral faces and by the top face, either with the ambient air or with other cells.

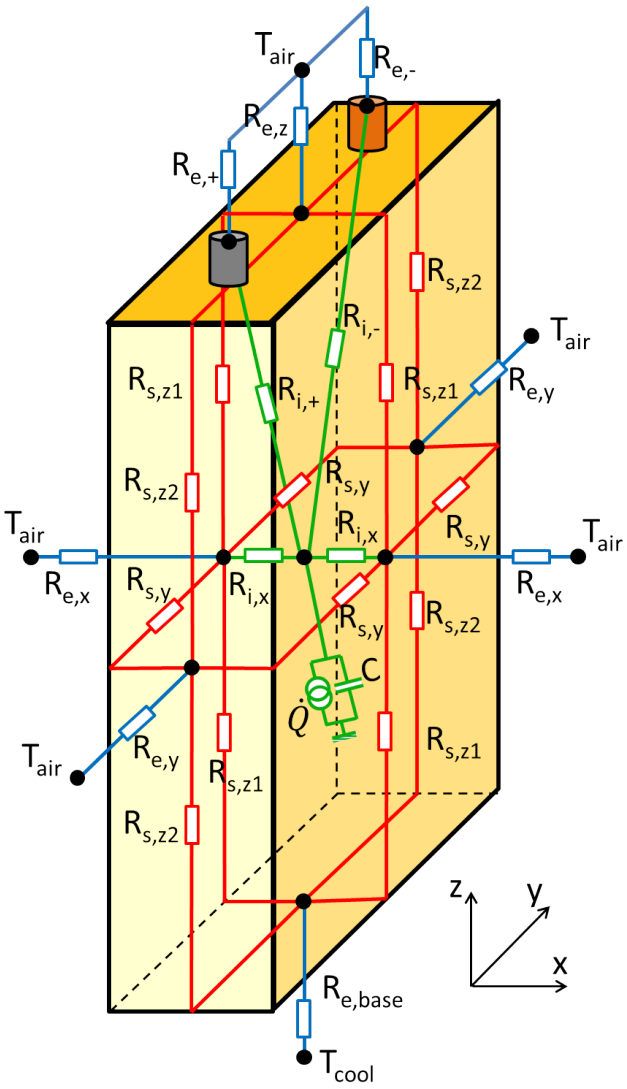

Figure 3: Lumped thermal model of a cell.

2.2. Thermal parameters characterization

The following work considers a battery pack central cell. In this case, heat mostly flows in the z direction, because of surrounding cells that are assumed to be at the same temperature. Those conditions are experienced while packing a cell with insulating materials on its upper (glass wool) and lateral faces ($10cm$ thick plates of polyurethane foam ($0.2W.m^{-1}.K^{-1}$)). Its base is placed on a cooling system (temperature-regulated system) (Figure 4a).

Values and determination methods of the different components of the thermal model are summarized in Table 1. Parameters are sorted by location and by type.

Heat generation: The heat source component is highly non linear. The design of the latter is treated in part three where it will be shown that its value depends on the current, the temperature and the SoC.

Heat capacity: In order to identify the heat capacity C, the battery was packed with insulating materials on every face (including the base). It is being heated by

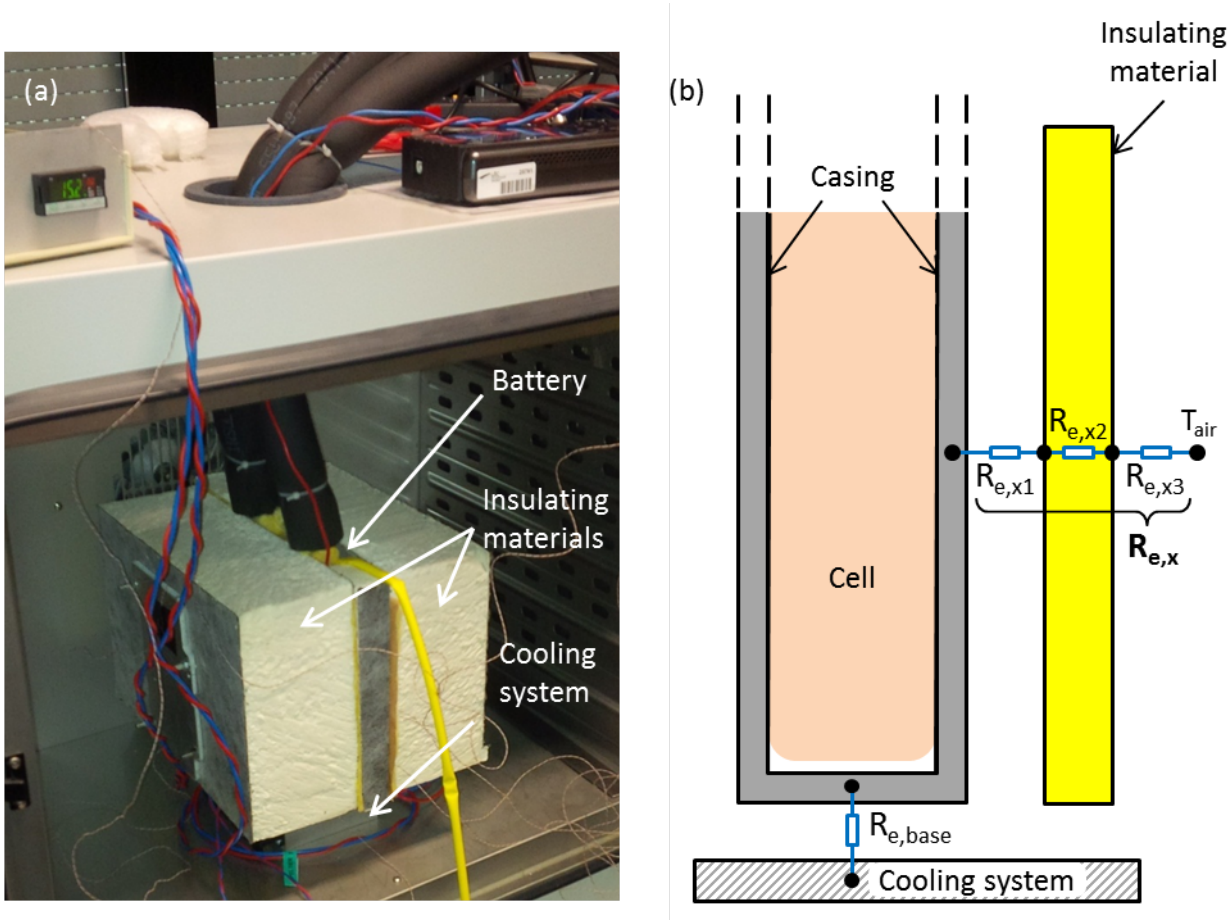

Figure 4: (a) Experimental setup approaching the battery-pack central-cell conditions and (b) details about the heat transfer resistances outside the casing.

	Value	**Evaluation**	**Equation**
$\dot{Q}$	Variable	Model	(5)
C	$1000\,J.K^{-1}$	Experimental	(1)
$R_{i,x}$	$0.8\,K.W^{-1}$	Experimental	(2)
$R_{i,+}$	$7.8\,K.W^{-1}$	Analytical	(3)
$R_{i,-}$	$8.0\,K.W^{-1}$	Analytical	(3)
$R_{s,y}$	$3.1\,K.W^{-1}$	Analytical	(3)
$R_{s,z1}$	$8.9\,K.W^{-1}$	Analytical	(3)
$R_{s,z2}$	$36.9\,K.W^{-1}$	Analytical	(3)
$R_{e,x}$	$140.9\,K.W^{-1}$	Analytical	(3) & (4)
$R_{e,y}$	$445.6\,K.W^{-1}$	Analytical	(3) & (4)
$R_{e,z}$	$90.7\,K.W^{-1}$	Analytical	(3) & (4)
$R_{e,+/-}$	$19.8\,K.W^{-1}$	Analytical	(3) & (4)
$R_{e,bot}$	$1.8\,K.W^{-1}$	Experimental	

Table 1: Values and determination methods of the different components of the thermal model

applying a $\pm$ 1C square current with a period of $20\,s$ (a 1C current fully discharges the battery in $1\,h$). The 20-second-long period has been chosen because it is very small compared to the thermal time constant of the cell. Thus, the average heat generation $\dot{Q}_{avg}$ can be used in a calculus instead of the instantaneous heat generation. This current solicitation has been chosen because it makes the $\dot{Q}_{avg}$ calculus simple and accurate. As the mean current is equal to zero, the mean reversible heat is also equal to zero. Thus, only electrical losses contribute to the cell heating *(see part three)*. They can be measured directly by :

- measuring the open circuit voltage U_{oc} before the beginning of the test (the cell being at the equilibrium) ;
- measuring the current I_{cell} and the cell voltage U_{cell} during the test.

At the beginning of the test, the internal temperature T_{in} increases by following a ramp. Consequently, the heat capacity can be determined using Equation (1) :

$$C = \frac{\dot{Q}_{avg}}{dT_{in}/dt} = \frac{(I_{cell}(U_{cell} - U_{oc}))_{avg}}{dT_{in}/dt} \quad (1)$$

From the calculated heat capacity, the specific heat was found to be $0.83\,J.g^{-1}.K^{-1}$. The latter is consistent with results found in literature [6].

Internal heat transfer in x direction: The cell internal resistance $R_{i,x}$ was experimentally obtained using the value of C and measurements made by a third party. Several thermocouples have been put inside (in its median plan) and outside a cell. The cell has been placed in a climatic chamber with no insulating material, heated by a full discharge and then rested. During the cell cooling, most of its heat is evacuated by its faces in x direction. Equation (2) can hence be derived.

$$R_{i,x} = \frac{\Delta T}{C\ \frac{dT_{in}/dt}{2}} = 0.8\ K.W^{-1} \tag{2}$$

ΔT is the temperature difference between the cell core T_{in} and the face in x direction. The heat flow running through $R_{i,x}$ is determined by the heat capacity "discharge".

Internal heat transfer toward terminals: Transfers between the core and the terminals ($R_{i,+}$ and $R_{i,-}$) are analytically determined using geometric features and Equation (3) [29], where L is the length, λ the thermal conductivity and S the section.

λ can be determined using the works of Lin *et al.* [6], by estimating the core component dimensions and calculating an equivalent thermal conductivity.

$$R = \frac{L}{\lambda\ S} \tag{3}$$

Heat transfer in the casing: Casing thermal resistances were also calculated using Equation (3), λ being the thermal conductivity of aluminum ($237\ W.m^{-1}.K^{-1}$). $R_{s,z1}$, $R_{s,z2}$, $R_{s,y}$ were obtained this way.

Heat transfer outside the casing: Thermal loss resistances from insulated faces to ambient air (Figure 4b) are considered as the sum of three terms. For instance, taking $R_{e,x}$:

- $R_{e,x1}$: contact resistance between the cell and the insulating material;
- $R_{e,x2}$: conduction through the insulating material;
- $R_{e,x3}$: convection between the insulating material surface and the ambient air.

Using typical values of contact resistance, $R_{e,x1}$ was found to be negligible compared to $R_{e,x2}$ and $R_{e,x3}$ [30]. $R_{e,x2}$ and $R_{e,x3}$ are determined using Equations (3) and (4) respectively. h is a transfer coefficient, which often needs to be determined experimentally [14]. In that case, convection has a minor impact on $R_{e,x}$ regarding $R_{e,x2}$. Therefore, the main objective is to determine a realistic value of h ($27\ W.m^{-2}.K^{-1}$)[10].

$$R = \frac{1}{h\ S} \tag{4}$$

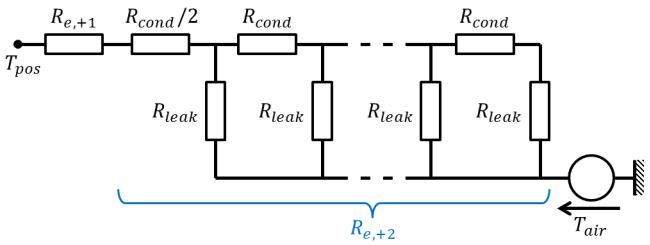

Figure 5: Power wires simple thermal model.

$R_{e,x}$ was found to be $140.9\ K.W^{-1}$ ($R_{e,x3}$ being estimated as $2.1\ K.W^{-1}$). The same calculation is applicable to $R_{e,y}$ and $R_{e,z}$. Radiation transfers are neglected, because of the relatively low temperature of the cell during function.

Heat transfer between terminals and ambient air: Thermal loss resistances from positive and negative terminals to ambient air are identical and considered as the sum of two terms. For instance, taking $R_{e,+}$:

- $R_{e,+1}$: contact resistance between the positive terminal and the power wire;
- $R_{e,+2}$: transfer between the end of the power wire and the ambient air;

$R_{e,+1}$ can be calculated using a typical surfacic conductance value of a copper-copper contact: $6.000\ W.m^{-1}.K^{-1}$ [30], leading to $1.7\ K.W^{-1}$.

$R_{e,+2}$ represents the heat transfer between the wire end and the ambient air. To calculate the corresponding thermal resistance, the wire has been discretized into 20 elements of 10 cm (Figure 5). Each of them is, on the one hand, connected to the adjacent elements by a conduction resistance R_{cond} (calculated using Equation (3)), and on the other hand, connected to the ambient air via a leakage thermal resistance R_{leak}, which is the sum of the conduction through the insulating materials (wire sheathing and isolating foam) and the convection to the ambient air (Equation (4)). Local heat capacitances and heat sources (electrical losses) have been neglected to simplify the calculus. For a wire longer than 1 m, the equivalent resistance $R_{e,+2}$ tends to be a constant value, being $18.1\ K.W^{-1}$. Hence, the value of $R_{e,x}$ is $19.8\ K.W^{-1}$.

Contact between cell and cooling system: Finally, the interfacial resistance $R_{e,bot}$, being the last unknown parameter, can be determined via an identification algorithm. The cell has been heated by a square current in the experimental setup shown by Figure 4a (same solicitation as for the heat capacity determination), with a thermocouple on its face in x direction. Its temperature has been recorded at the thermal steady state. Then, the value of $R_{e,bot}$ has been adjusted for the model to fit the experimental data. Hence, the latter is found to be equal to $1.8\ K.W^{-1}$.

3. Heat generation

Heat capacity and thermal resistances being determined, heat sources have now to be characterized to create a complete thermal model. They are highly variable as they depend on current, SoC, temperature and aging (the latter not being considered in this study). Inside any battery, four heat sources can be found : electrical losses, entropic heat, heat generated by side reaction(s) and heat of mixing [8]. Concerning the studied battery, side reactions are mostly aging reactions that are slow enough for their heat generation to be neglected. The heat of mixing is negative during the creation of concentration gradients and is positive when those gradients disappear (the sum being zero) [31]. Besides, its contribution to the cell heat generation is minor compared to electrical losses [32]. As a consequence, the heat of mixing has been neglected in the following model. Consequently, only entropic heat $\dot{Q}_{\Delta S}$ and electrical losses $\dot{Q}_{elec}$ are considered in total heat generation $\dot{Q}$ (Equation 5).

$$\dot{Q} = \dot{Q}_{elec} + \dot{Q}_{\Delta S} \tag{5}$$

3.1. Entropic heat (reversible heat)

There are structural changes within the electrodes as the cell is being charged or discharged. These changes can release or absorb some energy, resulting in heat generation or consumption. The corresponding physical quantity is the entropy variation ΔS, which only depends on SoC (within the operating temperature range). Equation (6) expresses the entropic heat generation $\dot{Q}_{\Delta S}$ as a function of the current I_{cell}, the inner temperature T_{in}, the entropy variation ΔS, the number of electrons exchanged n and the Faraday's constant F. Classically, the term $\Delta S/nF$ is replaced by the derivative of the open-circuit voltage with respect to temperature $\partial U_{oc}/\partial T$, which is more convenient to use.

$$\dot{Q}_{\Delta S} = I_{cell}\ T_{in}\ \frac{\Delta S}{nF} = I_{cell}\ T_{in}\ \frac{\partial U_{oc}}{\partial T} \tag{6}$$

The entropic heat modeling only needs the knowledge of $\partial U_{oc}/\partial T$, which is a function of the SoC and depends on the electrode types as well as on their concentrations [15, 33]. For this work, $\partial U_{oc}/\partial T$ has been evaluated during a specific test on a similar chemistry (Figure 6).

3.2. Electrical losses (irreversible heat)

The voltage drop during discharge (resp. increase during charge) corresponds to an irreversible transformation of electrical energy into heat. It is called the "overvoltage" ΔU and is defined as the difference between the cell voltage U_{cell} and the equilibrium open-circuit voltage U_{oc}. Hence, electrical losses are the product of the current I_{cell} and the overvoltage ΔU (Equation (7)).

$$\dot{Q}_{elec} = I_{cell} \times \Delta U = I_{cell}\ (U_{cell} - U_{oc}) \tag{7}$$

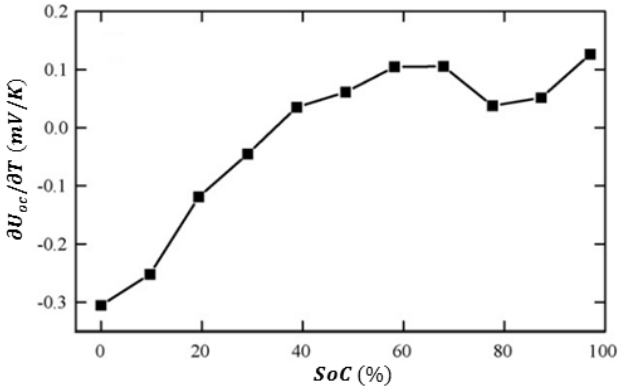

Figure 6: Derivative of open-circuit voltage with respect to the temperature ($LiFePO_4$/graphite 26650 battery, 2.3 Ah) [8].

Using Equation (7), electrical losses can thus be estimated during operation by :

- estimating U_{oc}. It depends on the SoC, the current direction (following a hysteresis cycle, which is about 10 mV large) [20, 27] and on the temperature (Figure 6);
- measuring U_{cell}, which depends on I_{cell}, time, T_{in} and on the SoC;
- measuring I_{cell}.

The overvoltage is caused by the voltage drop (or increase) in the cell internal resistances (current collectors and conductive additives around the active material) and by the cell polarization, due to diffusion (mass transport, with creation or relaxation of concentration gradients). The latter is a phenomenon that evolves in time and space within the electrodes and the electrolyte (3D). Seen from the cell terminals, the voltage and current are 1D, making the cell's electrical behavior quite complex to model.

For the calculus of the electrical losses, the overvoltage will be extracted from an electrical model. The latter is based on a Randles circuit which combines the two electrodes and electrolyte dynamics into one (Figure 7a). This classical model has been adapted to meet this study purposes. Double layer capacitance C_{dl} is neglected because it is related to a very quick dynamic (about 0.1s) compared to thermal phenomena dynamic (about 1000 s). Thus, the electrolyte resistance R_e and the charge transfer resistance R_{ct} can be considered as a unique "high frequency" resistance R_{HF} (Figure 7b). Warburg impedance Z_W is modeled by a series of n "low frequency" RC circuits.

Kuhn *et al.* [34] has shown that the RC parameters can be computed using only two parameters k_1 and k_2 (see Equations (8) and (9)).

$$R_{LF,i} = \frac{8k_1}{(2i-1)^2\pi^2} \quad with \quad i \in [1, ..., n] \tag{8}$$

$$C_{LF,i} = \frac{k_1}{2{k_2}^2} \quad with \quad i \in [1, ..., n] \tag{9}$$

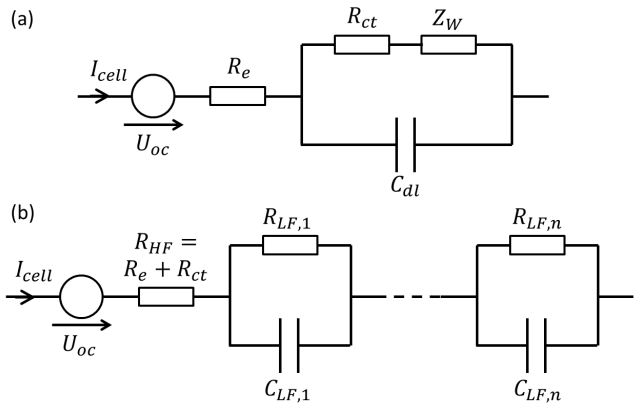

Figure 7: (a) Randles circuit and (b) model for electrical losses.

Model parameters have been experimentally determined using GITT experiments (Galvanostatic Intermittent Titration Technique). The cell has been put into a climatic chamber, without any insulating materials in order to control its temperature. It has been charged and discharged by short pulses separated by rest periods (Figure 8). The latter allow the cell to return to the chamber temperature and its concentration gradients to vanish. From a strict point of view, the battery should rest several hours for it to be at the equilibrium. This time has been shortened for the purpose of limiting the characterization tests duration. 30-minute-long rest period has been chosen as a good trade-off between test durations and precision for U_{oc} determination ($\pm$ 10 mV).

GITT tests have been conducted at different current rates (from C/5 to 2C) and different chamber temperatures (from 5°C to 45°C). The goal is to create look-up tables for charge and discharge as function of the current, the temperature and the SoC. The temperature dependency on the electrical parameters is part of the coupling between the thermal and heat generation models (Figure 2).

Voltage measurements of a constant charge at C/2 are presented in Figure 8 as a function of the SoC. After estimating the cell's temperature to be about 32°C during this charge, a GITT test has been run at this temperature for comparison. Interestingly, there is a good correspondence between voltage of the constant charge and the envelope of the GITT test. This correspondence has been verified for other current rates (in charge and discharge) and temperature values, with similar results. To simplify the parameter determination, the battery overvoltage is assumed to reach a quasi-steady state at the pulse ends (capacitors are considered as open-circuits but resistances may still change due to SoC or temperature evolution). This corresponds to a diffusion phenomenon which appears according to bounded conditions. Gagneur *et al.* [24] also modeled a $LiFePO_4$/graphite cell and came to the same conclusion concerning the diffusion phenomena.

Details about parameter determination are reported in Figure 8. The open-circuit voltage U_{oc} is directly measured from the voltage at the ends of each relaxation period. The following parameters are extracted from each pulse overvoltage. The quasi-steady state resistance R_{QS} is the result of the pulse final-overvoltage divided by the current. k_1 can be calculated from R_{HF} and R_{QS} values (Equation (10)). R_{HF} value is predetermined from the quick voltage change at the beginning of the pulse (within 0.1 s and 1 s). Finally, R_{HF} and k_2 values are determined through an optimization routine, using the overvoltage data (least square method).

$$\begin{aligned} R_{QS} &= R_{HF} + \sum_{i=1}^{n} R_{LF,i} \\ &= R_{HF} + k_1 \sum_{i=1}^{n} \frac{8}{(2i-1)^2\pi^2} \end{aligned} \tag{10}$$

GITT test data have been fitted for different number of RC circuits. Using only $n = 1$ RC circuit, the root-mean-square error (RMSE) remains below 1 mV. This is acceptable for modeling heat generation, as the cell overvoltage is about 100 mV during nominal function.

Temperature changes during GITT pulses should be considered in order to improve the accuracy of the parameter determination. Thus, R_{HF} and R_{QS} are determined respectively for T_1 and T_2 (see Figure 8) which are respectively the cell temperatures at the beginning and at the end of the pulse. T_2 is estimated from T_1, using the test data. GITT pulses are short compared to the cell thermal time-constant in the climatic chamber. Therefore, the cell can be assumed to operate in adiabatic conditions. This results in a temperature rise that can be derived from the generated thermal energy Q_{pulse} and the thermal capacity C_{th} (Equation (11)). Q_{pulse} is calculated using Equation (5). The irreversible losses are extracted from the overvoltage data (see Equation (7)). To simplify the reversible heat calculus (Equation (6)), the temperature is assumed to be equal to T_1 during the whole pulse.

$$T_2 - T_1 = \frac{Q_{pulse}}{C_{th}} = \frac{1}{C_{th}} \int \dot{Q} dt \tag{11}$$

Accounting for the temperature evolution during parameter determination is particularly important at high current or at low temperature because of the heat generation rate significant increase (e.g. for a GITT test at 2C and for $T_1 = 5$ °C, T_2 is about 11 °C).

4. Experimental validation

After the cell being modeled, tests were performed in pack conditions (Figure 4a). The ambient air temperature is 25 °C and the cooling system has been set to 15 °C. The cell is considered to be in its thermal steady state before being:

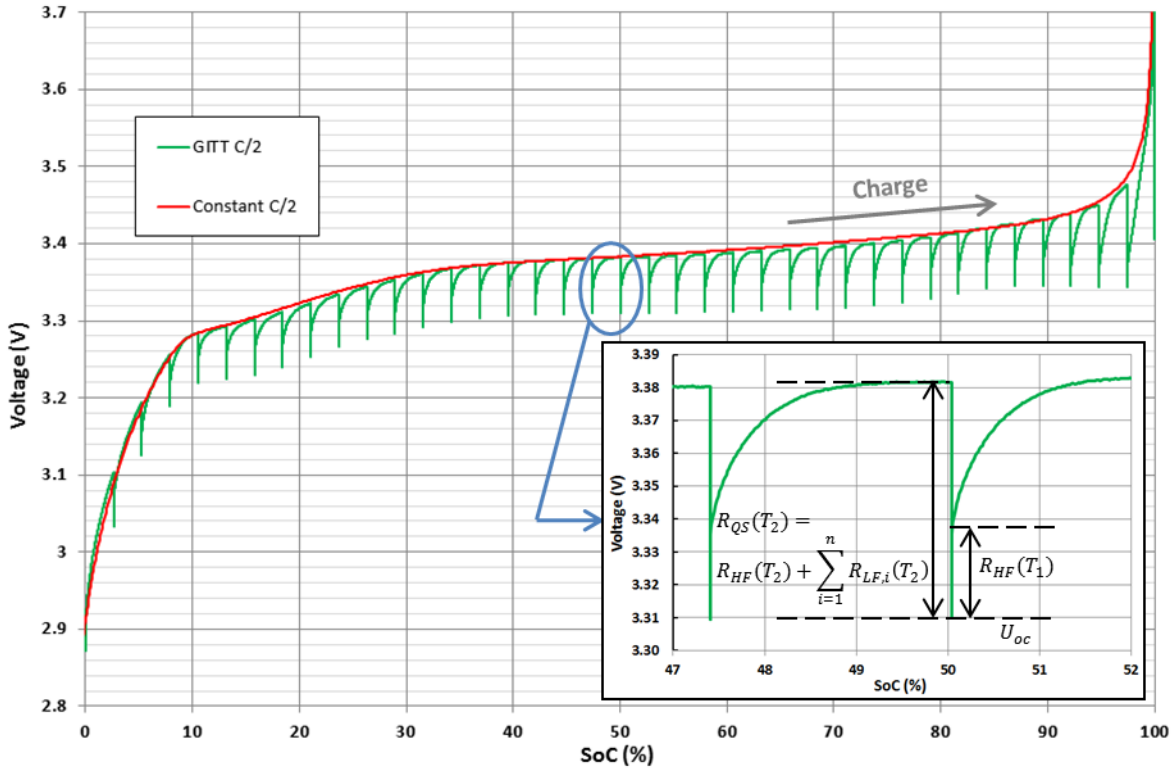

Figure 8: C/2 charge under constant current (estimated to be 32 °C) and using GITT method (thermal chamber at the same temperature). Details about parameter determination.

- fully discharged with a 2C current (in about 30 min);
- rested for 30 min;
- fully charged with a C/2 current, using the CCCV method (in about 2 h);
- rested for 1 h.

At each calculation step, electrical losses are computed via the electrical model using the current profile, the estimated cell internal temperature and the SoC. Total heat generation is calculated thanks to Equation (5). The result is used by the thermal model for calculating the temperatures in the following step. Experimental voltage and current have been recorded to estimate the experimental electrical losses and compare the latter to the model estimation (see part 3.2 and Figure 9).

On Figure 9a, it can be seen that the 2C discharge generates more heat than the C/2 charge, mostly because of electrical losses (irreversible heat). For ease of reading, a zoom has been made on the charge phase (Figure 9b). During the whole test, three electrical losses' peaks can be observed. The first peak, at the beginning of the discharge phase ($t \approx 0h$), is due to the high values of resistances at low temperature. These resistances decrease rapidly while the temperature rises. The two following peaks ($t \approx 0.5h$ and $3h$) are due to the "low frequency" resistance R_{LF} increase at the discharge and charge ends. During most of the charge phase, the cell's temperature is quite constant and so are the electrical losses. This validation cycle is interesting because it highlights the three influences of current, temperature and SoC on electrical losses.

As for the entropic heat, it has a secondary but significant contribution during the discharge phase. It consumes some heat at the beginning and generates a heat peak of several watts at the end. During the charge phase, the entropic heat is of the same order of magnitude than electrical losses. As a result, it has a strong influence on the cell's total heat generation. Interestingly, heat generation is negative at the beginning of the charge: this would means that more heat is being consumed by chemical reactions than being generated by electrical losses.

The error between measured and simulated electrical losses is reported in Figure 10 (black curve). Since the absolute error is maximum for the 2C discharge, only the latter has been represented. The RMSE during discharge is 1.4 W. It is mainly due to an underestimation of the electrical losses. The latter result can be explained by the shortness of the rest periods during GITT tests, which lead to an underestimation of the overvoltage ΔU. The maximum error, found at the end of discharge, is caused by the rapid variation of U_{oc} at low SoC which makes the overvoltage more difficult to estimate and the electrical parameters much more complex to determine. The same effect can be observed near SoC 100% during the charge phase.

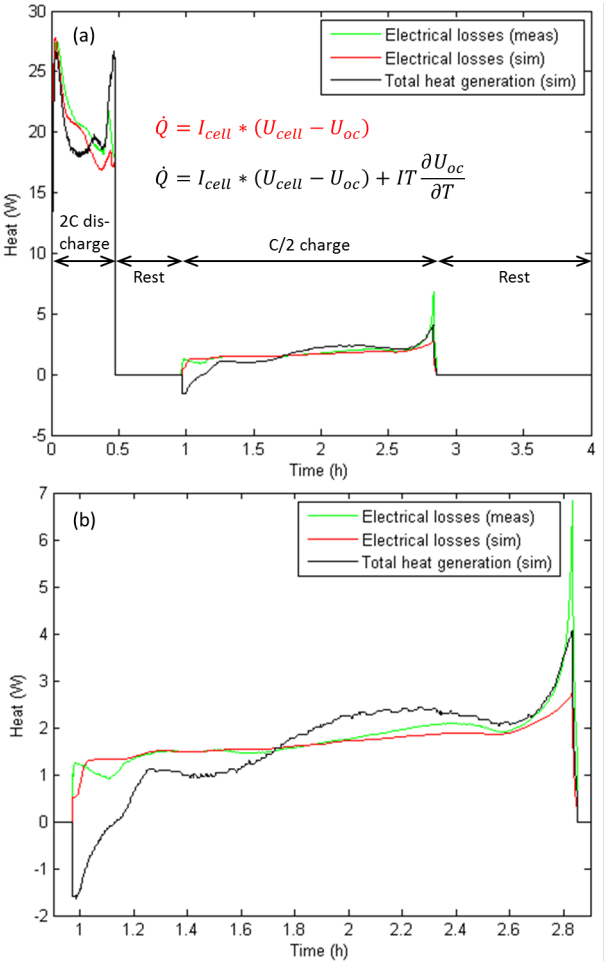

Figure 9: (a) Heat generated and evacuated and (b) zoom on the heat generation during charge.

Another simulation has been run using different electrical parameters. The latter have been determined using the proposed method but the cell's temperature is assumed to be constant during characterization (red curve on Figure 10). The RMSE is here 2.4 W (71% higher than with the proposed method). It can be seen that the difference between the errors is temperature-dependent. In particular, the error is more than doubled for room temperature (20-25 °C) and it approaches zero near 40 °C. The comparison of the 2 curves highlights the interest of considering the cell heating during characterization.

Temperature evolutions are represented in Figure 11a for the:

- T_{core}: cell core (simulated);
- T_{surf}: face in x direction (measured and simulated);
- T_{base}: cell base (simulated);
- T_{air}: ambient air (measured);
- T_{cool}: cooling system (measured).

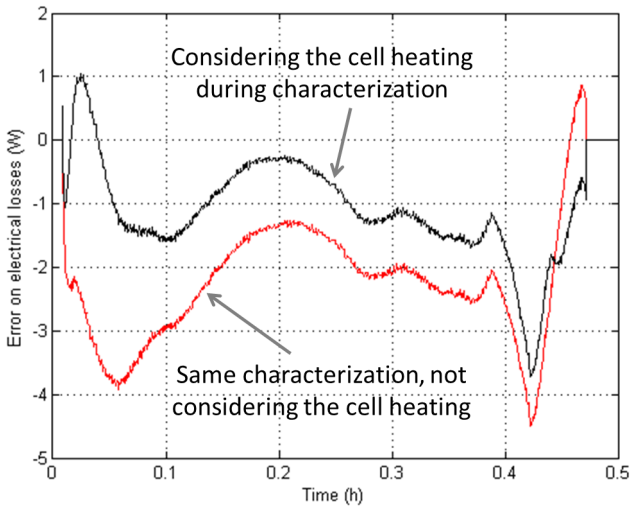

Figure 10: Error between measured electrical losses and simulations during the 2C discharge. Simulations use electrical parameters determined with or without considering the cell heating during characterization.

This test is interesting because it puts the cell in thermal steady and transient states. Due to the large amount of heat generated during 2C discharge regarding the expelled heat, the cell's surface temperature quickly rises from 18 °C to 42 °C. As this rise is well simulated, it indicates that the value of the estimated heat capacity is accurate. During the temperatures decrease and while the thermal steady state is around 2.5 h, measurements were in good agreement with simulation. This reflects the good estimation of thermal resistances.

Simulation shows a difference of 2.5 °C between T_{surf} and T_{core}. The latter is quite small, whereas the cell is well-cooled and is hence able to stay in acceptable temperature ranges. As for the casing, T_{base} is about 18 °C colder than T_{surf} at the end of the discharge. This difference implies that the cell is indeed cooled by its base through its casing. Thus, the latter is very important for cooling performances in this configuration. T_{base} reaches a 9 °C difference with the cooling system due to the interfacial thermal resistance. This confirms the sensibility of the system cooling-performances to this interface and, as a result, strengthens the dependence of the simulation quality on this resistance determination.

Heat flows evacuated by the cooling system and through insulating materials leakages and power wires have been computed by the thermal model and reported in Figure 11b. Power wires appear to have a significant contribution to the thermal behavior (about 20% of the evacuated heat at the end of the discharge phase). This is not surprising since good electrical conductors are also good thermal conductors. Besides, at least 73% of the total evacuated heat flows through the cooling system. This confirms the capacity of the experimental setup to cool down the cell by its base, as it is the case in the studied battery pack.

The heat generation model gives good results, as both

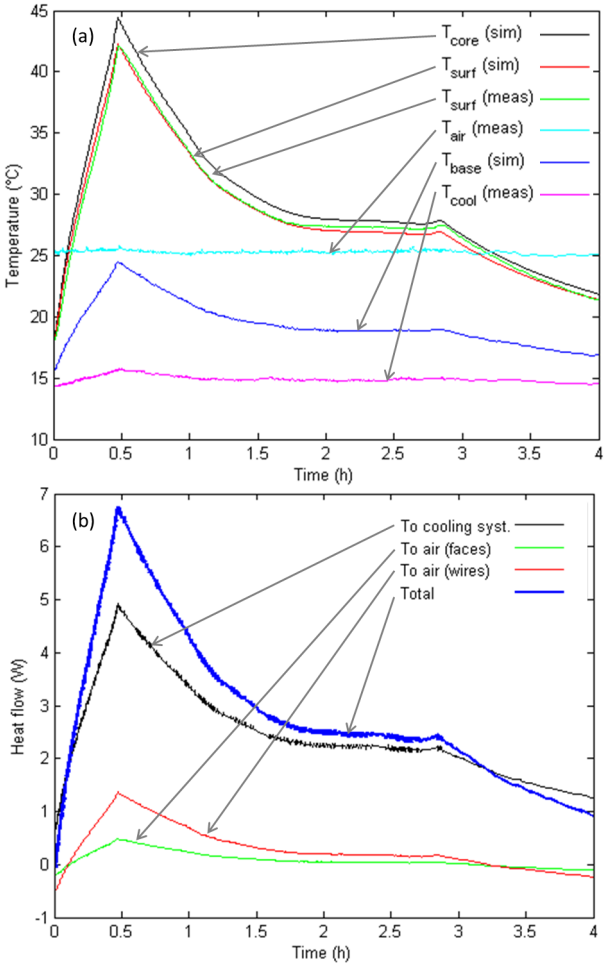

Figure 11: (a) Temperature evolutions and (b) computed heat flows to ambient air and to support.

electrical losses and temperature evolutions are in accordance with measurements. The precision of the proposed coupled models is better than 1°C.

5. Conclusion

A thermal model for a large prismatic lithium cell has been presented. It represents the thermal behavior of a battery-pack central cell, which is bound to be the hottest one. Thus, the proposed study can be used for a whole battery-pack temperature-monitoring. A heat generation model has also been proposed, considering entropic heat and electrical losses. Some methods have been proposed to determine both model parameters. The coupled simulations have been experimentally validated through a discharge-charge cycle. They are able to represent typical thermal phenomena and give reliable information on cell key-temperatures.

The electrical model used for electrical losses and its parameter determination method are based on the assumption of a quasi-steady state, reached after a few minutes under constant current. Its components depend on temperature, SoC and current. Whereas a single RC circuit was used for the diffusion phenomenon, the proposed model gives good results for long constant-current simulations. A significant improvement of the electrical losses estimation has been achieved by considering the battery heating during characterization which is due to heat generation during current pulses. The latter has been estimated via the coupled thermal and heat generation models.

The proposed coupled models are well-suited for embedded applications, such as a BMS or for an off-line usage, such as a battery pack thermal-design tool. They are also suitable for larger objects (such as a whole battery pack) as several cell models can be easily interconnected. To do so, thermal transfers between cells and the battery pack environment should be characterized, as well as inner convection transfers.

Acknowledgment

The authors would like to thank the ANRT (2012/0257) for its financial support, E4V for its participation in the study, Yves Chabre for his scientific support.

References

[1] M. Gholizadeh, F. R. Salmasi, Estimation of State of Charge, Unknown Nonlinearities, and State of Health of a Lithium-Ion Battery Based on a Comprehensive Unobservable Model, IEEE Transactions on Industrial Electronics 61 (3) (2014) 1335–1344.

[2] H. Rahimi-Eichi, F. Baronti, M.-Y. Chow, Online Adaptive Parameter Identification and State-of-Charge Coestimation for Lithium-Polymer Battery Cells, IEEE Transactions on Industrial Electronics 61 (4) (2014) 2053–2061.

[3] A. Smyshlyaev, M. Krstic, N. Chaturvedi, J. Ahmed, A. Kojic, PDE model for thermal dynamics of a large Li-ion battery pack, Am. Control Conf. (ACC), IEEE (2011) 959–964.

[4] X. Hu, S. Asgari, S. Lin, S. Stanton, W. Lian, A linear parameter-varying model for HEV/EV battery thermal modeling, Energy Convers. Congr. Expo. (ECCE), IEEE (2012) 1643–1649.

[5] C. Mi, B. Li, D. Buck, N. Ota, Advanced Electro-Thermal Modeling of Lithium-Ion Battery System for Hybrid Electric Vehicle Applications, Vehicle Power and Propulsion Conference (VPPC), IEEE (2007) 107–111.

[6] C. Lin, K. Chen, F. Sun, Research on thermo-physical properties identification and thermal analysis of EV Li-ion battery, Veh. Power Propuls. Conf. (VPPC), IEEE (2009) 1643–1648.

[7] A. Pruteanu, B. V. Florean, G. M. Moraru, R. C. Ciobanu, Development of a thermal simulation and testing model for a superior lithium-ion-polymer battery, Optim. Electr. Electron. Equip. (OPTIM), IEEE (2012) 947–952.

[8] C. Forgez, D. Vinh Do, G. Friedrich, M. Morcrette, C. Delacourt, Thermal modeling of a cylindrical $LiFePO_4$/graphite lithium-ion battery, J. Power Sources 195 (9) (2010) 2961–2968.

[9] C. Alaoui, Solid-State Thermal Management for Lithium-Ion EV Batteries, IEEE Trans. Veh. Technol. 62 (1) (2013) 98–107.

[10] K&K Associates, Thermal Network Modeling Handbook, K&K Associates, Westminster, 1999.

[11] E. Barsoukov, J. H. Jang, H. Lee, Thermal impedance spectroscopy for Li-ion batteries using heat-pulse response analysis, J. Power Sources 109 (2) (2002) 313–320.

[12] M. Fleckenstein, S. Fischer, O. Bohlen, B. Bäker, Thermal Impedance Spectroscopy - A method for the thermal characterization of high power battery cells, Journal of Power Sources 223 (2013) 259–267.

[13] X. Lin, H. E. Perez, S. Mohan, J. B. Siegel, A. G. Stefanopoulou, Y. Ding, M. P. Castanier, A lumped-parameter electro-thermal model for cylindrical batteries, Journal of Power Sources 257 (2014) 1–11.

[14] X. Lin, H. E. Perez, J. B. Siegel, A. G. Stefanopoulou, Y. Li, R. D. Anderson, Y. Ding, M. P. Castanier, Online Parameterization of Lumped Thermal Dynamics in Cylindrical Lithium Ion Batteries for Core Temperature Estimation and Health Monitoring, IEEE Trans. Control Syst. Technol. PP (99) (2012) 1–11.

[15] Y. F. Reynier, R. Yazami, B. Fultz, Thermodynamics of Lithium Intercalation into Graphites and Disordered Carbons, J. Electrochem. Soc. 151 (3) (2004) A422–A426.

[16] V. V. Viswanathan, D. Choi, D. Wang, W. Xu, S. Towne, R. E. Williford, J.-G. Zhang, J. Liu, Z. Yang, Effect of entropy change of lithium intercalation in cathodes and anodes on Li-ion battery thermal management, J. Power Sources 195 (11) (2010) 3720–3729.

[17] J. P. Schmidt, A. Weber, E. Ivers-Tiffée, A novel and precise measuring method for the entropy of lithium-ion cells: ΔS via electrothermal impedance spectroscopy, Electrochim. Acta 137 (2014) 311–319.

[18] K. E. Thomas, J. Newman, Thermal Modeling of Porous Insertion Electrodes, Journal of The Electrochemical Society 150 (2) (2003) A176.

[19] M. Farkhondeh, M. Safari, M. Pritzker, M. Fowler, T. Han, J. Wang, C. Delacourt, Full-Range Simulation of a Commercial $LiFePO_4$ Electrode Accounting for Bulk and Surface Effects: A Comparative Analysis, J. Electrochem. Soc. 161 (3) (2013) A201–A212.

[20] W. Dreyer, J. Jamnik, C. Guhlke, R. Huth, J. Moskon, M. Gaberscek, The thermodynamic origin of hysteresis in insertion batteries., Nat. Mater. 9 (2010) 1–6.

[21] K. Onda, T. Ohshima, M. Nakayama, K. Fukuda, T. Araki, Thermal behavior of small lithium-ion battery during rapid charge and discharge cycles, J. Power Sources 158 (1) (2006) 535–542.

[22] M. Fleckenstein, O. Bohlen, M. A. Roscher, B. Bäker, Current density and state of charge inhomogeneities in Li-ion battery cells with $LiFePO_4$ as cathode material due to temperature gradients, J. Power Sources 196 (10) (2011) 4769–4778.

[23] N. Watrin, H. Ostermann, B. Blunier, A. Miraoui, Multiphysical Lithium-Based Battery Model for Use in State-of-Charge Determination, IEEE Trans. Veh. Technol. 61 (8) (2012) 3420–3429.

[24] L. Gagneur, A. Driemeyer-Franco, C. Forgez, G. Friedrich, Modeling of the diffusion phenomenon in a lithium-ion cell using frequency or time domain identification, Microelectron. Reliab. 53 (6) (2013) 784–796.

[25] K. Murashko, J. Pyrhonen, L. Laurila, Three-Dimensional Thermal Model of a Lithium Ion Battery for Hybrid Mobile Working Machines: Determination of the Model Parameters in a Pouch Cell, IEEE Trans. Energy Convers. 28 (2) (2013) 335–343.

[26] E. Kuhn, C. Forgez, G. Friedrich, Modeling diffusive phenomena using non integer derivatives, Eur. Phys. J. Appl. Phys. 25 (3) (2004) 183–190.

[27] M. A. Roscher, D. U. Sauer, Dynamic electric behavior and open-circuit-voltage modeling of $LiFePO_4$-based lithium ion secondary batteries, J. Power Sources 196 (1) (2011) 331–336.

[28] J. P. Schmidt, P. Berg, M. Schönleber, A. Weber, E. Ivers-Tiffée, The distribution of relaxation times as basis for generalized time-domain models for Li-ion batteries, Journal of Power Sources 221 (2013) 70–77.

[29] S. Chowdhury, P. K. Baski, A simple lumped parameter thermal model for electrical machine of TEFC design, Power Electron. Drives Energy Syst. Power India, IEEE (2010) 1–7.

[30] Y. Bertin, Refroidissement des machines électriques tournantes, Tech. l'ingénieur (1999) 1–22.

[31] K. E. Thomas, J. Newman, Heats of mixing and of entropy in porous insertion electrodes, Journal of Power Sources 119-121 (2003) 844–849.

[32] K. Chen, G. Unsworth, X. Li, Measurements of heat generation in prismatic Li-ion batteries, Journal of Power Sources 261 (2014) 28–37.

[33] R. E. Williford, V. V. Viswanathan, J.-G. Zhang, Effects of entropy changes in anodes and cathodes on the thermal behavior of lithium ion batteries, J. Power Sources 189 (1) (2009) 101–107.

[34] E. Kuhn, C. Forgez, P. Lagonotte, G. Friedrich, Modelling Ni-MH battery using Cauer and Foster structures, J. Power Sources 158 (2) (2006) 1490–1497.